

## **GROUP THEORY BASED DESIGN OF ISOTROPIC NEGATIVE REFRACTIVE INDEX METAMATERIALS**

**N. Wongkasem and A. Akyurtlu**

Department of Electrical and Computer Engineering  
University of Massachusetts Lowell  
MA 01854, USA

**K. A. Marx**

Center for Intelligent Biomaterials, Department of Chemistry  
University of Massachusetts Lowell  
MA 01854, USA

**Abstract**—Novel isotropic planar and three-dimensional negative refractive index (NRI) metamaterial (MTM) designs consisting of periodically arranged cross structures are developed in the terahertz (THz) frequency regime using group theory. The novel designs not only avoid magnetoelectric coupling but also enable a simplified fabrication process. Using Finite-difference Time-Domain (FDTD) simulations, the design exhibits an NRI passband which is in good agreement with the S-parameters obtained from Fresnel's equation. Cross-polarized fields are used to characterize the magnetoelectric coupling mechanism and determination of material properties of the medium via group theory aid in the characterization of the isotropy of the structure. Numerical simulations of a wedge composed of the proposed metamaterials prove the negative refractive index of the models.

### **1. INTRODUCTION**

A negative index metamaterial (NIM) is an artificial material with a negative index of refraction. This property leads to many promising applications such as perfect lenses [1], subwavelength resonators [2], and novel optical filters. Typically, the structures utilized for NIM are bi-anisotropic [3], having a broken spatial symmetry, which results in magnetoelectric coupling having directional dependences.

Furthermore, many of the previously designed single negative and NIM structures [4–6] are anisotropic, i.e., their properties are directionally dependent. Since these extra properties can destroy the desired negative index (NI) behavior [7] and transmission properties, it is necessary to design isotropic NIMs with no cross-coupling.

There has been an effort in previous years to design isotropic NIMs. A split ring resonator (SRR) [8] was originally proposed to provide negative permeability that can be used in the construction of NIMs. Most SRRs suffer from anisotropy [3, 9] and also show evidence of cross-coupling [3, 10–11]. Recently, there has been some work devoted to developing isotropic SRRs [3, 9, 12–14]. By combining artificial dielectrics with magnetic metamaterials, two-dimensional [15] and three-dimensional [7] isotropic left-handed metamaterials have also been reported. Marques et al. [15] introduced an arrangement of a broadside-coupled SRR (BC-SRRs) array and metallic plates, while Koschny et al. [7] used fully symmetric multigap single-ring SRRs and crossing continuous wires for three-dimensional NIM. These models, based on the split-ring and wire design, contain two separate structures. The BC-SRRs also show evidence of cross-coupling. The 3D design of [7] successfully eliminates the cross polarization terms; however, their 25 piece construction is difficult to fabricate.

In this paper, using group theory, we propose novel isotropic planar and three-dimensional negative index metamaterial models, consisting of “cross” structures. The proposed material also has the added advantage of not possessing any cross-coupling and due to its simple structure, is also easy to fabricate. Group theory is used to derive material properties which are then used to prove the isotropy and lack of coupling within the material. Moreover, the co- and cross-polarized fields are characterized to gain insight into the magneto-electric coupling mechanisms. The proof of the negative refractive index of the proposed structure, using a wedge model [16] of the novel design, is also demonstrated. Analysis and results are shown in the terahertz (THz) frequency regime, although this approach can be scaled to other frequency regimes (microwave to optical).

## 2. GROUP THEORY

Group theory, a formalism used to classify the symmetry of molecules, has been used in a limited fashion to identify the isotropy of magnetic resonators of metamaterials [13, 14]. In chemistry, the symmetry of molecules and solids has been characterized by Group Theory in order to develop an understanding of bonding and physical properties. As an example, Group Theory has been used to characterize many

molecules' bonding and non-bonding molecular orbitals, which has led to descriptions of allowed and disallowed electronic transitions between molecular orbitals within those molecules that have been subsequently confirmed by spectroscopic experiments. Beyond its application in Chemistry, it has been used to classify functions according to how the structures behave when the symmetry operations of a point group are performed upon them [17]. The symmetry of a structure can be described in terms of the complete collection of symmetry operations it possesses. Regardless of the number of operations, five main operations will always be used [18]. These are termed: (1) identity, " $E$ ", (2) rotation (sometimes called proper rotation), " $C_n$ ", (3) reflection, " $\sigma$ ", (4) inversion, " $i$ ", and (5) a two-part operation called rotation-reflection (or improper rotation), " $S_n$ ". The operations are performed on: (1) the object itself, (2) a line (rotation axis or proper axis), (3) a plane (reflection plane or mirror plane), (4) a point (inversion center or center of symmetry), and (5) a line (improper axis or alternating axis). All the corresponding symmetry elements will pass through a common point at the center of the structure. Based on these operations, the point groups can be categorized into nonaxial groups ( $C_n, D_n, C_{nv}, C_{nh}, D_{nh}, D_{nd}, S_n$ ) cubic groups and linear groups ( $C_{\infty v}, D_{\infty h}$ ) [18, 19].

After the structure is categorized into a group, an electromagnetic (EM) basis can be assigned to the structure by applying a wave polarization concept. By investigating and transforming this basis according to the symmetries of the group, the EM mode, spatial independence, magnetoelectric and cross-couplings can be established.

### 3. ISOTROPIC APPROACH

Negative index metamaterials can be obtained through a combination of negative permeability and negative permittivity materials. Many NIMs (from GHz to THz frequencies) have used SRR/wire composites [20–23]. Artificial dielectrics, which include the wire structure [8] as an example, normally generate exceptionally low cross-polarization [14]. On the other hand, a basis set of the SRR is in the  $C_{2v}$  point group [13] has been shown to be bi-anisotropic. Hence, both the negative permeability artificial medium (i.e., the SRR) and the NIM that is designed with it, show the effects of bi-isotropy and bi-anisotropy [3]. Bi-anisotropic media have a broken spatial symmetry. The constitutive relations for the bi-anisotropic materials are governed by the following four medium dyadics [24] two co-polarization dyadics, permittivity  $\bar{\bar{\epsilon}}$  and permeability  $\bar{\bar{\mu}}$ , and two cross-polarization (magnetoelectric) dyadics  $\bar{\bar{\xi}}$  and  $\bar{\bar{\zeta}}$  [25]. Without magnetoelectric coupling,  $\bar{\bar{\xi}}$  and  $\bar{\bar{\zeta}}$  vanish

in anisotropic materials. For a bi-isotropic (BI) medium, the dyadics are multiples of the unit dyadic, and therefore they can be expressed in terms of four scalar coefficients  $\varepsilon$ ,  $\mu$ ,  $\xi$ , and  $\zeta$ . The BI media are magnetoelectric, but are not sensitive to field direction. The simplest form of media is an isotropic material which has only an  $\varepsilon$  and  $\mu$  with no differential spatial direction.

In this section, we will apply group theory to the design of the isotropic NIM using artificial dielectrics, composed of capacitively loaded strips, CLS, [26] and magnetic resonators [13]. The isotropic magnetic metamaterial (MTM) will be modified and combined with the CLS to obtain a NIM.

### 3.1. Isotropy of Artificial Dielectric

The CLS can be categorized in an orthorhombic type ( $D_{2h}$  point group). Fig. 1 shows the transmission coefficients of the discontinuous wire (rod) and the CLS. The stopbands appear at 1440 GHz and 920 GHz, respectively. The linewidth and length of the basic rod structure are 8 and 88 micron. Adding extra capacitance with 56 micron length bars, CLS has a lower stopband.

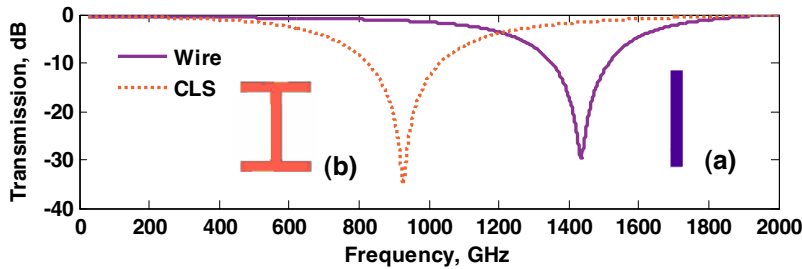


**Figure 1.** (a) discontinuous wire (solid). (b) CLS (dotted).

With the  $D_{2h}$  point group, the symmetry of the CLS contains eight elements:  $[E, C_2(z), C_2(y), C_2(x), i, \sigma(xy), \sigma(xz), \sigma(yz)]$  as illustrated in Fig. 2.

The character table for the  $D_{2h}$  point group is shown in Table 1.

All possible sets of characters (irreducible representations) for a given point group are shown in this character table. The columns are labeled according to the number and type of operations forming each class. The labels of the irreducible representations are  $A$  (or  $B$ ) for one-dimensional representations. Two-dimensional representations are labeled  $E$ , and three-dimensional ones are labeled  $T$ . When inversion symmetry is present, it is customary to use “ $g$ ” and “ $u$ ” as subscripts

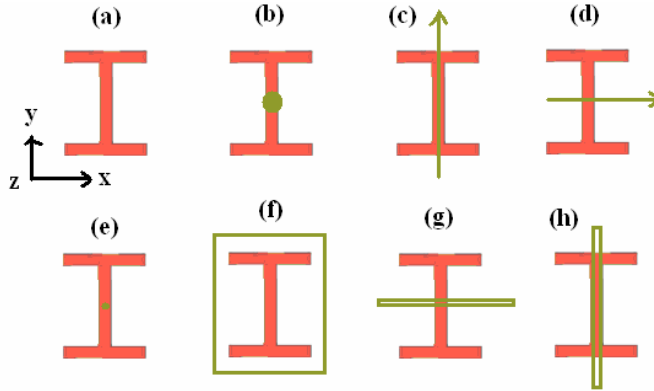


**Figure 2.** Eight symmetry elements of CLS (a) Identity,  $E$ , (b)–(d) symmetry axes in  $z$ ,  $y$ , and  $x$  by rotating 180 degrees named as  $C_2(z)$ ,  $C_2(y)$  and  $C_2(x)$ , (e) inversion center,  $i$ , (f)–(h) mirror plane symmetries for  $x$ - $y$ ,  $x$ - $z$ , and  $y$ - $z$  planes named as  $\sigma(xy)$ ,  $\sigma(xz)$ ,  $\sigma(yz)$ .

**Table 1.** Character table for the  $D_{2h}$  point group.

$D_{2h}$	$E$	$C_2(z)$	$C_2(y)$	$C_2(x)$	$i$	$\sigma(xy)$	$\sigma(xz)$	$\sigma(yz)$	Linear	Quadratic
$A_g$	1	1	1	1	1	1	1	1		$x^2, y^2, z^2$
$B_{1g}$	1	1	-1	-1	1	1	-1	-1	$R_z$	$xy$
$B_{2g}$	1	-1	1	-1	1	-1	1	-1	$R_y$	$xz$
$B_{3g}$	1	-1	-1	1	1	-1	-1	1	$R_x$	$yz$
$A_u$	1	1	1	1	-1	-1	-1	-1		
$B_{1u}$	1	1	-1	-1	-1	-1	1	1	$z$	
$B_{2u}$	1	-1	1	-1	-1	1	-1	1	$y$	
$B_{3u}$	1	-1	-1	1	-1	1	1	-1	$x$	

for even and odd numbers, respectively [18]. The other columns list the coordinates, quadratic forms of coordinates, and rotations.

Some representations reveal the wave polarization which can be seen from the second to last column in Table 1.  $B_{1u}$ ,  $B_{2u}$ , and  $B_{3u}$  show the polarized light along the  $z$ ,  $y$ , and  $x$  axis, respectively, which means  $B_{1u}$ ,  $B_{2u}$ ,  $B_{3u}$  have the electric field in the  $z$ ,  $y$ , and  $x$  directions. On the other hand,  $B_{1g}$ ,  $B_{2g}$ ,  $B_{3g}$  have the magnetic field polarized along

the  $z$ ,  $y$ , and  $x$  axis, respectively, according to the rotation function  $R_\alpha$ . However, there is only a certain number of distinct ways in which a function can behave when subjected to the symmetry operation of a particular point group. We can generate the representation for the CLS for the  $D_{2h}$  point group by the concept of wave polarization together with the molecular orbital group theory (MOGT). First, arrows will be marked to represent directions of currents due to an external electric field and then we will find the representation of a set of the orbitals for each of the symmetry operations.

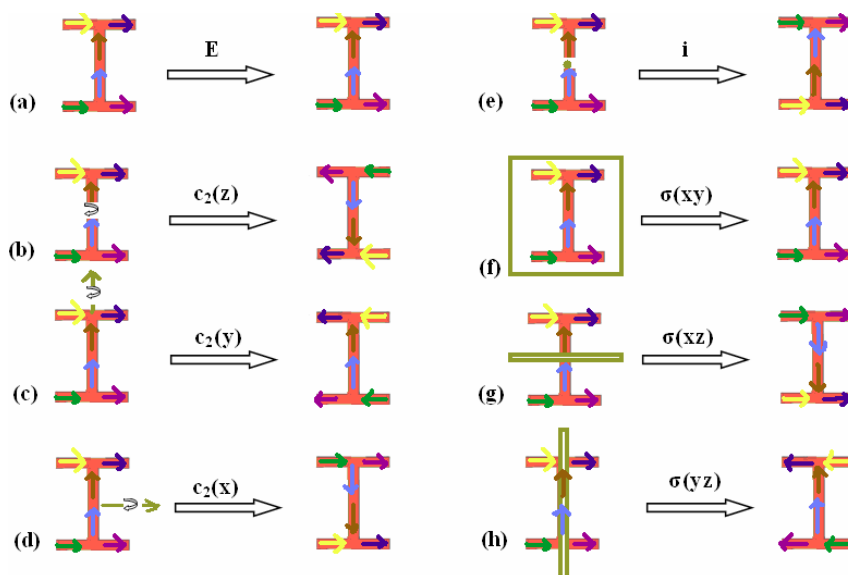


**Figure 3.** Behavior of CLS under the symmetry elements (a)  $E$ , (b)  $C_2(z)$ , (c)  $C_2(y)$ , (d)  $C_2(x)$ , (e)  $i$ , (f)  $\sigma(xy)$ , (g)  $\sigma(xz)$ , and (h)  $\sigma(yz)$ .

Under the eight symmetry operations illustrated in Fig. 3 acting upon the CLS structure, the polarized light behavior can be observed by the location and direction of the arrows. If the arrow is in the same direction following the symmetry operation, we designate it as “1”, and if the arrow is still in the same location but in the opposite direction, it is designated as “-1”. If the arrow does not remain in the same location following the symmetry operation, it is designated as “0”. [27]. For the identity symmetry in Fig. 3(a), the arrows are unchanged so the character for each is +1 giving a total of +6. None of the arrows is the same after applying the  $C_2(z)$ ,  $C_2(x)$ ,  $i$ ,  $\sigma(xy)$ ,  $\sigma(xz)$  symmetries, giving 0 for a total. And, there are two arrows which are unchanged in  $C_2(y)$ ,  $\sigma(yz)$  giving a total of +2. The numbers of each

symmetry element of the CLS are then:

Now we can assign a basis set to the model and see how this basis set transforms under the symmetry operations to represent an electrical activity of the structure. The basis set can be calculated by:

$$n_i = \frac{1}{h} \sum_c g_c \chi_i \chi_r \quad (1)$$

where  $h$  is the order of the group ( $h = 8$  in this case), and is the total number of symmetry operations [28]. The summation is over all types (classes) of symmetry elements in the group. For each type of symmetry element, the product of three numbers is required:  $g_c$  is the number of symmetry elements of that type (1<sup>st</sup> row of Table 1),  $\chi_i$  represents the characters for the irreducible representation in question (Table 1), and  $\chi_r$  refers to the characters for the irreducible representation (Table 2). Using Equation (1), the representation reduces to  $2A_g, B_{1g}, B_{2u}$ , and  $B_{3u}$  or  $\Gamma_{CLS} = 2A_g + B_{1g} + 2B_{2u} + B_{3u}$ . Thus, there are three linear modes that include a magnetic mode ( $B_{1g}$ ),  $H_z$ , and two electric modes ( $B_{2g}$  and  $B_{3g}$ ),  $E_y$ , and  $E_x$ . With no occurrences of the rotation and linear basis functions being together, this can confirm that there is neither a direction dependence nor magnetoelectric term. Therefore, the CLS categorized in  $D_{2h}$  point group can be straightforwardly adjusted to fit in any isotropic NIM designs. Note that the number of irreducible representatives should come out as zero or as a positive integer; if it does not, then either the formula has been used incorrectly or the reducible representation has been generated incorrectly or both.

**Table 2.** Irreducible representations for CLS.

$D_{2h}$	$E$	$C_2(z)$	$C_2(y)$	$C_2(x)$	$i$	$\sigma$ ( $xy$ )	$\sigma$ ( $xz$ )	$\sigma$ ( $yz$ )
$\Gamma_{CLS}$	6	0	2	0	0	6	0	2

The CLS of the same dimension as mentioned before in Fig. 1 will be used to construct the novel isotropic NIM. According to the location of the stopband, we can presume that the negative index pass band of the NIM should be in the stopband interval of the CLS.

### 3.2. Artificial Magnetic Material Design

The planar magnetic MTM, introduced by Padilla [13], is shown in Fig. 4(c). This structure is not sensitive to field direction, does not

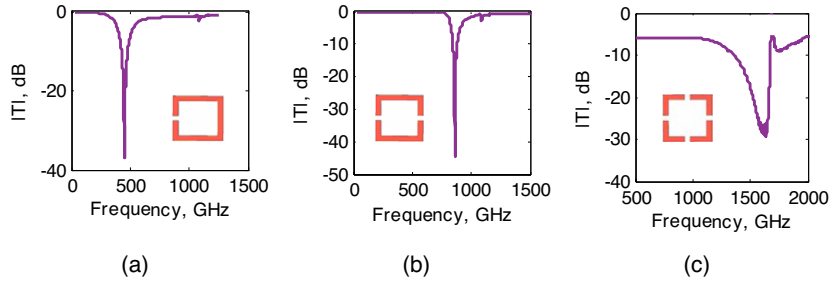


**Figure 4.** SRR with (a) one gap, (b) two gaps, and (c) four gaps.

possess magnetoelectric coupling and is therefore isotropic. Four gaps are presented to increase the symmetry. However, the transmission property ( $S$  parameters) of such designs change from that of the regular SRR according to the specific modifications made- e.g., breaking the structure resulting in extra gaps. Thus, the study of this structure is required in designing the NIM. The extra gaps act like capacitors in series, leading to a considerable lowering of the total capacitance and thus to an increase of  $\omega_m$ . The transmission coefficients of three SRRs which have one, two and four gaps are illustrated in Fig. 4. The magnetic resonances appear at 430 GHz, 880 GHz, and 1,680 GHz, respectively, where the width and length of all the SRRs are 88 micron, and the line width and gap are both 8 micron. These results are consistent with those of Kafesaki et al. [12] and show that the resonance frequency of an  $n$ -gap SRR is approximately “ $n$ ” times higher than that from a one-gap SRR. Although the resonance frequency may be adjusted by decreasing the gap size or adding extra bars to increase the capacitance, the strength of the magnetic resonance and the width of the “ $\mu < 0$ ” regime may be affected by the modification. Therefore, this shift of the resonance, due to the additional introduction of gaps, must be considered when the structure is modified in the NIM design.

### 3.3. Isotropic NIM by Group Theory

For a two-dimensional NI structure, our first design, the two separate structures (electric and magnetic response structures) will be joined to produce only a single piece. This helps to reduce not only the couplings which may diminish or even destroy the NI behavior, but also any potential misalignment in the manufacturing process which becomes a factor when two sets of structures are involved. To ensure the elimination of the off-diagonal permeability and permittivity terms and two cross-polarization (magnetoelectric)

dyadics in the response functions, one should consider point groups with no appearance of linear basis functions and rotational function  $R_\alpha$  at the same time and with little or no occurrences of linear functions. The point group  $D_{4h}$  (tetragonal) will be used. This sixteenth order tetragonal point group has sixteen symmetry elements  $[E, 2C_4, C_2, 2C_2', 2C_2'', i, 2S_4, \sigma_h, 2\sigma_v, 2\sigma_d]$ . No linear basis functions and rotational function occurs in the same irreducible representative. In Fig. 5, the  $D_{4h}$  symmetry is represented by three structures: a stereograph, a rudimentary molecule structure, and the novel one piece isotropic NIM, a “cross” model. The cross, in Fig. 5(c), actually, combines a CLS and a flipped CLS. Note that a location of the NI passband can be adjusted by changing the gap size between the bars. Yet, the gaps can not be too wide, which will cause a high magnetic response and thus may be too high to correspond to the electric response.

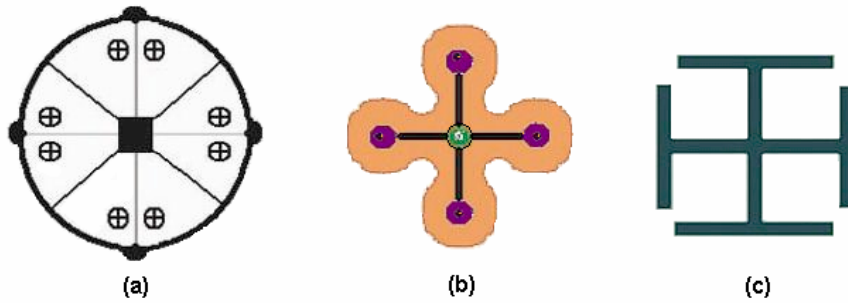


**Figure 5.** (a) Stereograph and (b) Molecule structure of the  $D_{4h}$  point group (c) Planar cross model.

Following the same steps as for the CLS, the irreducible representations of the planar cross model can be obtained as shown in Table 3.

**Table 3.** Irreducible representations for cross.

$D_{4h}$	$E$	$2C_4$	$C_2$	$2C_2'$	$2C_2''$	$i$	$2S_4$	$\sigma_h$	$2\sigma_v$	$2\sigma_d$
$\Gamma_{CROSS}$	8	0	0	0	0	0	0	8	0	0

Using the reduction formula (1), the cross model is represented as:  $\Gamma_{CROSS} = A_{1g} + A_{2g} + B_{1g} + B_{2g} + 2E_u$ . With the only magnetic mode of  $A_{2g}$  and the identical electric fields  $E_x$  and  $E_y$  along the  $x$

and  $y$  axes of the electric mode in the  $E_u$  mode, neither extra coupling nor direction dependence terms occur in this planar cross model.

#### 4. NUMERICAL RESULTS AND VALIDATION OF ISOTROPIC NIM

A Finite Difference Time Domain (FDTD) model with periodic boundary conditions, was implemented to examine the transmission property of the cross structure [29]. The normalized electric fields with respect to the number of time steps of co- ( $E_z$ ) and cross- ( $E_\phi$ ) electric field components are shown in Fig. 6. The incident and the reflected fields are collected at port 1 while the transmitted wave is gathered at port 2.

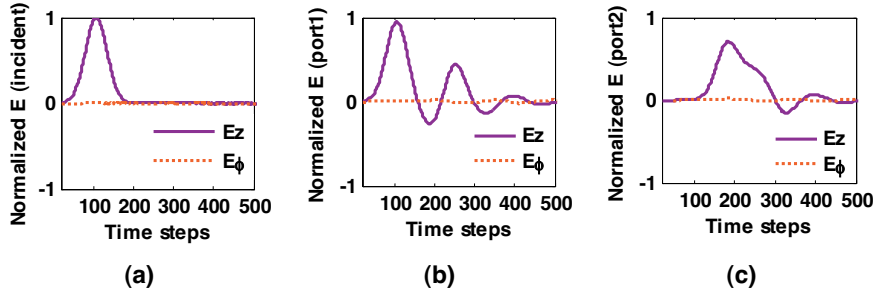


**Figure 6.** Normalized co- $E$  component (solid line) and cross- $E$  component 1 (dotted line) of (a) incident field, (b) port 1, and (c) port 2.

The incident electric field along the  $z$ -axis (solid line in Fig. 6(a)) is a Gaussian excitation, launched at port 1. As expected, the cross-polarized incident field (dotted line in Fig. 6(a)) is zero for all time. The co-polarized  $E$ -field component (solid line in Fig. 6(b)) at port 1, with 95.4% of the starting peak intensity, combines the incident and reflected waves in the core direction. The transmitted field at port 2 (in Fig. 6(c)) has 71.0% of peak intensity at its highest point. Conversely, both transmitted and reflected waves of the cross-polarized  $E$ -field component are extraordinarily low with the highest values only at 2.1% and 1.9% of peak intensity, respectively (dotted lines in Fig. 6(b) and (c)).

The low values of the cross-polarized  $E$ -field component,  $E_\phi$ , signify that there is no cross-polarized transmission coefficient at all frequencies, as predicted. The negative refractive index band is predicted to be centered at 950 GHz and can be seen in the transmission

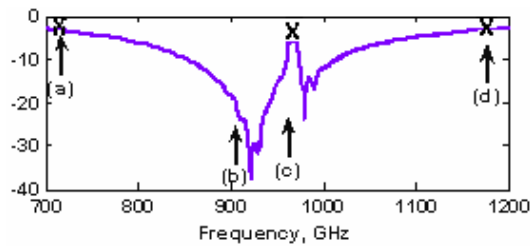


**Figure 7.** Transmission coefficient of the cross model with a 8 micron gap.

coefficient of the cross model shown in Fig. 7. Note that a location of the NI passband can be adjusted by changing the gap size between the bars. Yet, the gaps cannot be too wide, which will cause a high magnetic response and thus may be too high to correspond to the electric response.

In order to validate the existence of an NI band, a FDTD simulation on a wedge-shaped structure was constructed at the predicted NIM band (950 GHz, point c in Fig. 7) and at 3 other frequencies which are outside of this band, namely: 700 GHz, 900 GHz, and 1200 GHz (as shown in Fig. 7 as points (a), (b), and (d) respectively). We use a simulation of the Snell's law experiment on a wedge-shaped structure [16], which is one of the most intuitive verifications of negative index metamaterials. The base and the height of the wedge model have six and three sets of the cross structure, respectively. The number of the crosses decreases by two in the consecutive rows to construct the 26 degree angle. According to the perfect magnetic conductor (PMC) set up on the top and bottom, only one layer of the MTMs on the direction of propagation is required. The other two sides where the MTMs are placed have perfect electric conductor (PEC) boundaries. The remaining boundaries are set by using a perfectly matched layer (PML) boundary condition to absorb the radiated fields. Fig. 8 demonstrates the propagation directions of the NIM in 26° wedge-shaped model. Fig. 8(a)–(b) illustrates the positive index values at 700 GHz and 1200 GHz, a stop band at 900 GHz, and the negative index at 950 GHz.

The gray lines are drawn to set the wedge surface and the line normal to that surface. The white lines demonstrate the direction of the wave after propagating through the 26° wedge metamaterials. Fig. 8(a) and (d) show the propagating wave with positive angles (positive refractive index) before and after the NI band at 700, and 1200 GHz, respectively. Corresponding to the stopband, indicated by

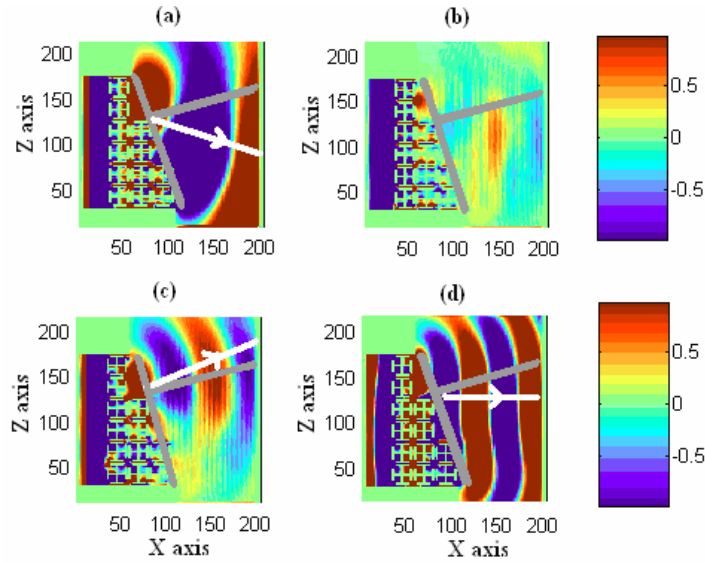


**Figure 8.** Propagation directions in Wedge-shaped models: (a) Wedge model with positive index at 700 GHz (b) Wedge model with a stop band at 900 GHz (c) Wedge model with negative index at 950 GHz and (d) Wedge model with a positive index at 1200 GHz.

the second arrow in Fig. 7, there is almost no transmission at 900 GHz in Fig. 8(b). The wedge model illustrates the reversal of Snell's Law as a result of the negative index (transmission angle =  $-18^\circ$ ) in Fig. 8(c). Using Snell's law, the index of refraction of the cross model can be calculated as,  $n = -0.705 \pm 0.1$ . In order to validate the correct retrieval of the index of refraction at frequencies at points, (a), (c), and (d), we calculate the analytical form of the S21 parameter [30] using the retrieved indices of refraction and compare with the FDTD results, as shown in Fig. 7. The analytical values of S21 are plotted in Fig. 7 at point (a), (c) and (d), indicated by 'x'. The results, at 700, 950, and 1200 GHz, respectively, show good agreement, i.e., less than  $-5$  dB, confirming the correct characterization of our model.

## 5. THREE-DIMENSIONAL NIM

Among four cubic point group candidates i.e.,  $T_h$ ,  $T_d$ ,  $I_h$ , and  $O_h$ , which are free from magnetoelectric response [13], we propose the  $O_h$  symmetry or cubic with 48 orders, one of the simplest possible symmetries for our 3D model. The character table of the  $O_h$  point

group is shown in Table 4.

**Table 4.** Character table for the  $O_h$  point group.

$O_h$	$E$	$8C_3$	$6C_2$	$6C_4$	$3C_2'$	$i$	$6S_4$	$8S_6$	$3\sigma_h$	$6\sigma_d$	Linear	Quadratic
$A_{1g}$	1	1	1	1	1	1	1	1	1	1		$x^2+y^2+z^2 (=r^2)$
$A_{2g}$	1	1	-1	-1	1	1	-1	1	1	-1		
$E_g$	2	-1	0	0	2	2	0	-1	2	0		$(3z^2-r^2, x^2-y^2)$
$T_{1g}$	3	0	-1	1	-1	3	1	0	-1	-1	$(R_x, R_y, R_z)$	
$T_{2g}$	3	0	1	-1	-1	3	-1	0	-1	1		$(xy, yz, zx)$
$A_{1u}$	1	1	1	1	1	-1	-1	-1	-1	-1		
$A_{2u}$	1	1	-1	-1	1	-1	1	-1	-1	1		
$E_u$	2	-1	0	0	2	-2	0	1	-2	0		
$T_{1u}$	3	0	-1	1	-1	-3	-1	0	1	1	$(x, y, z)$	
$T_{2u}$	3	0	1	-1	-1	-3	1	0	1	-1		

Three structures which all have the symmetry of this  $O_h$  point group are shown in Fig. 9. Fig. 9(a) shows a 3D cubic object. Fig. 9(b) shows a rudimentary representation of the 3D structure of the molecule  $SF_6$ , where the  $S$  atom occurs in the center bonded to the 6 external F ligand atoms. Finally, in Fig. 9(c) the isotropic 3D cross model is shown.

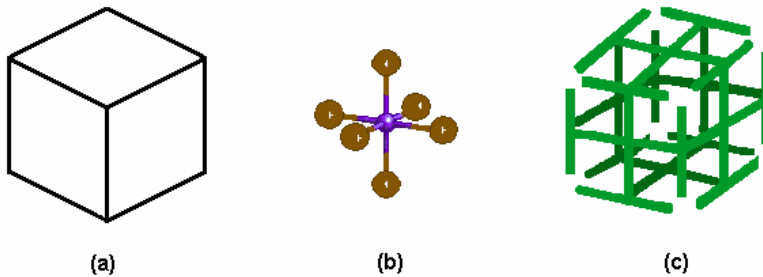


**Figure 9.** (a) 3D object (b) Molecule structure of the  $O_h$  point group (c) Isotropic cubic array of cross model.

The 3D cross model is represented by:  $\Gamma_{3D-CROSS} = 1A_{1g} + 1A_{2g} + 2E_g + 1T_{1g} + 1T_{2g} + 2T_{1u} + 2T_{2u}$ . There are four three-dimensional representations:  $T_{1g}, T_{2g}, T_{1u}$ , and  $T_{2u}$ . However, only  $T_{1g}$  and  $T_{1u}$  independently provide the magnetic and electric fields

polarized along the three axes.  $T_{1g}$  states three identical magnetic fields in three dimensions while  $T_{1u}$  presents three identical electric fields. Hence, the 3D cross model does not generate either the two co-polarization dyrics (off-diagonal permittivity and permeability terms) or the two cross-polarization (magnetoelectric) dyrics. Because it has directional independence with no magnetoelectric coupling, the structure is confirmed to be isotropic.

## 6. CONCLUSION

We utilize molecular symmetry and group theory to identify directional dependence and magnetoelectric coupling based on the occurrence of the four material parameter dyrics of the metamaterials in the THz regime. We propose novel isotropic negative index metamaterial models for both the planar and three-dimensional versions. Transmission coefficients, co- and cross-polarization terms from FDTD simulations are used to validate the design. The simulated wedge model is used to validate the negative index of refraction of the designed structures. Values of the  $S$ -parameters obtained from analytical equations using the extracted index of refraction values from the wedge studies, further support the transmission properties and the extraction method.

## REFERENCES

1. Pendry, J. B., "Negative refraction makes a perfect lens," *Phys. Rev. Lett.*, Vol. 85, 3966–3969, 2000.
2. Engheta, N., "An idea for thin, subwavelength cavity resonators using metamaterials with negative permittivity and permeability," *IEEE Antennas and Wireless Propagation Letters*, Vol. 1, No. 1, 10–13, 2002.
3. Marqués, R., F. Medina, and R. Rafii-El-Idrissi, "Role of bianisotropy in negative permeability and left-handed metamaterials," *Phys. Rev. B.*, Vol. 65, 144440, Apr. 2002.
4. Yen, T. J., W. J. Padilla, N. Fang, D. C. Vier, D. R. Smith, J. B. Pendry, D. N. Basov, and X. Zhang, "Terahertz magnetic response from artificial materials," *Science*, Vol. 303, 1494–1496, 2004.
5. Linden, S., C. Enkrich, M. Wegener, J. Zhou, T. Koschny, and C. M. Soukoulis, "Magnetic response of metamaterials at 100 terahertz," *Science*, Vol. 306, 1351–1353, 2004.
6. Aydin, K., K. Guven, M. Kafesaki, L. Zhang, C. M. Soukoulis, and E. Ozbay, "Experimental observation of true left-handed

- transmission peaks in metamaterials,” *Optics Letters*, Vol. 29, No. 22, 2623–2625, Nov. 2004.
7. Koschny, Th., L. Zhang, and C. M. Soukoulis, “Isotropic three-dimensional left-handed metamaterials,” *Phys. Rev. B.*, Vol. 71, No. 12, 121103, 2005.
  8. Pendry, J. B., A. J. Holden, D. J. Robbins, and W. J. Stewart, “Magnetism from conductors and enhanced nonlinear phenomena,” *IEEE Trans. Microwave Theory Tech.*, Vol. 47, No. 11, 2075–2084, 1999.
  9. García-García, J., F. Martín, J. D. Baena, R. Marqués, and L. Jelinek, “On the resonances and polarizabilities of split ring resonators,” *J. Appl. Phys.*, Vol. 98, No. 3, 033103, 2005.
  10. Gay-Balmaz, P., C. Maccio, and O. J. F. Martin, “Microwire arrays with plasmonic response at microwave frequencies,” *Appl. Phys. Lett.*, Vol. 81, No. 15, 2896–2898, 2002.
  11. Katsarakis, N., T. Koschny, M. Kafesaki, E. N. Economou, and C. M. Soukoulis, “Electric coupling to the magnetic resonance of split ring resonators,” *Appl. Phys. Lett.*, Vol. 84, No. 15, 2943–2945, 2004.
  12. Kafesaki, M., Th. Koschny, R. S. Penciu, T. F. Gundogdu, E. N. Economou, and C. M. Soukoulis, “Left-handed metamaterials: detailed numerical studies of the transmission properties,” *J. Opt. A: Pure Appl. Opt.*, No. 7, S12–S22, 2005.
  13. Padilla, W. J., “Group theoretical description of artificial magnetic metamaterials utilized for negative index refraction,” <http://xxx.lanl.gov/abs/cond-mat/0508307>.
  14. Baena, J. D., L. Jelinek, R. Marqués, and J. Zehentner, “Electrically small isotropic three-dimensional magnetic resonators for metamaterial design,” *Appl. Phys. Lett.*, Vol. 88, 134108, 2006.
  15. Marqués, R., J. Martel, F. Mesa, and F. Medina, “A new 2D isotropic left-handed metamaterial design: theory and experiment,” *Microwave and Opt. Tech. Lett.*, Vol. 35, 405, 2002.
  16. Shelby, R., D. R. Smith, and S. Schultz, “Experimental verification of a negative index of refraction,” *Science*, Vol. 292, 77, 2001.

17. Ferraro, J. R., *Introductory Group Theory*, Plenum Press, New York, USA, 1969.
18. Carter, R. L., *Molecular Symmetry and Group Theory*, John Wiley & Sons, New York, USA, 1998.
19. Hatfield, W. E. and W. E. Parker, *Symmetry in Chemical Bonding and Structure*, Charles E. Merrill, Ohio, USA, 1974.
20. Smith, D. R., W. J. Padilla, D. C. Vier, S. C. Nemat-Nasser, and S. Schultz, "A composite medium with simultaneously negative permeability and permittivity," *Phys. Rev. Lett.*, Vol. 84, 4184–4187, 2000.
21. Moss, C. D., T. M. Grzegorzczuk, Y. Zhang, and J. A. Kong, "Numerical studies of left-handed metamaterials," *PIER*, Vol. 35, 316–333, 2002.
22. Katsarakis, N., T. Koschny, M. Kafesaki, E. N. Economou, E. Ozbay, and C. M. Soukoulis, "Left- and right-handed transmission peaks near the magnetic resonance frequency in composite metamaterials," *Phys. Rev. B.*, Vol. 70, 201101(R), 2004.
23. Zhang, S., W. Fan, N. C. Panoiu, K. J. Malloy, R. M. Osgood, and S. R. J. Brueck, "Experimental demonstration of near-infrared negative-index metamaterials," *Phys. Rev. Lett.*, Vol. 95, 137404, 2005.
24. Lindell, I. V., et al., *Electromagnetic Waves in Chiral and Bi-Isotropic Media*, Artech House, Boston, 1994.
25. Sihvola, A., *Electromagnetic Mixing Formulas and Applications*, T. J. Internation, Padstow, Cornwall, 1999.
26. Ziolkowski, R. W., "Design, fabrication, and testing of double negative metamaterials," *IEEE Trans. Antennas and Propagat.*, Vol. 51, No. 7, 1516–1529, 2003.
27. Bridgeman, A., <http://www.hull.ac.uk/php/chsajb/symmetry/>
28. Kettle, S. F. A., *Symmetry and Structure*, John Wiley & Sons, West Sussex, England, 1995.
29. Wongkasem, N., A. Akyurtlu, J. Li, A. Tibolt, Z. Kang, and W. D. Goodhue, "Computational and experimental analysis of thz double negative metamaterials," Special Session on "Smart EM materials and applications," *2005 IEEE AP-S International Symposium and USNC/URSI National Radio Science Meeting*, Washington, DC, July 3–8, 2005.
30. Jenkins, F. A. and H. E. White, *Fundamentals of Optics*, 4E, McGraw-Hill, 1976.